APPENDIX B

Publication P3

Repo A.-K., Niemenmaa A., Arkkio A. Estimating circuit models for a deep-bar induction motor using time harmonic finite element analysis. *Proceedings – International Conference in Electrical Machines*, Crete, Greece, September 2006, No. 614, 6 p.

Estimating circuit models for a deep-bar induction motor using time harmonic finite element analysis

Anna-Kaisa Repo, Asko Niemenmaa, and Antero Arkkio

***Abstract*—A method for estimating equivalent circuit models for deep-bar induction motor is presented. The method is based on the time-harmonic finite element analysis (FEA). The parameters of the studied motor depend strongly on the frequency and a single-cage equivalent circuit with constant parameters predicts the torque only at the same operation point where the parameters are defined. In the presented paper, the rotor is modelled with multiple branches and the same circuit model is capable of depicting a wider operation range of the motor.**

***Index Terms*—finite element analysis, parameter estimation, equivalent circuit models**

I. Introduction

THE time-stepping finite-element analysis is accurate and widely applied method in the study and simulation of electrical machines. Electrical machines usually operate in connection with control circuits, power electronics, components of electrical grid and mechanics causing a complex interaction. The computation capacity often limits the use of comprehensive models, and a simpler analytical model for the machine is required in many applications.

The basic single-cage equivalent circuit model with constant parameters is able to model the behaviour of the machine only at certain operation point. Because of the skin effect in the rotor bars, the parameters of the circuit model depend on the frequency. The values for the rotor resistance and leakage inductance vary the most. Several proposals have been made in order to include the skin effect into the circuit model, for example [1], [2]. Usually one or more additional rotor branches are included into the basic model, while the physical interpretation for the parameters is still preserved.

In the proposed paper, a systematic method for extracting the equivalent circuit parameters from the two-dimensional time-harmonic FEA is presented. For the analytical model, the number of additional branches can be chosen depending on the requirements of the application.

The authors are with the Laboratory of Electromechanics, Helsinki University of Technology, FI-02015 TKK, Finland (email: anna-kaisa.repo@tkk.fi; asko.niemenmaa@tkk.fi; antero.arkkio@tkk.fi)

II. Method of Analysis

A. Two-dimensional time-harmonic model

A radial-flux cage induction motor is studied assuming a two-dimensional magnetic vector potential $\boldsymbol{A}$ and current density $\boldsymbol{J}$

$$\begin{aligned}\boldsymbol{A} &= A(x,y,t)\mathbf{e}_z \\ \boldsymbol{J} &= J(x,y,t)\mathbf{e}_z\end{aligned}. \tag{1}$$

The z-axis is in the direction of the shaft of the machine. Assuming sinusoidal time variation, phasor variables are used for the field solution. The stator frequency is equal to the supply frequency ω_s. The rotor frequency is the slip frequency $s\omega_s$. The rotor is stationary, i.e. the effects of motion are modelled by assuming the slip frequency in the rotor, only. After these assumptions, the equation for the magnetic vector potential is

$$\nabla\times(\nu_{\mathrm{eff}}\nabla\times\underline{\boldsymbol{A}}) = \underline{\boldsymbol{J}} \tag{2}$$

where ν_{eff} is an effective permeability [3] and $\underline{\boldsymbol{A}}$ is the vector-potential phasor. This two-dimensional time-harmonic model can be used for the core region of a radial-flux machine but it does not model properly the magnetic field or winding connections in the end-winding space. The end effects are taken into account approximately by coupling the field equation with the circuit equations of the windings and using end-winding impedances. Winding currents or potentials or both of them are used as additional variables. For instance, the circuit equation for a stator phase is

$$\underline{u}_{\mathrm{n}}^{\mathrm{s}} = \left(R_{\mathrm{n}}^{\mathrm{s}} + \mathrm{j}\omega L_{\mathrm{n}}^{\mathrm{s}}\right)\underline{i}_{\mathrm{n}} + \mathrm{j}\omega\sum_{\mathrm{i}}\beta_{\mathrm{ni}}\frac{N_{\mathrm{ni}}\ell}{S_{\mathrm{ni}}}\int_{S_{\mathrm{ni}}}\underline{\boldsymbol{A}}\cdot\mathrm{d}\boldsymbol{S} \tag{3}$$

where $R_{\mathrm{n}}^{\mathrm{s}}$ and $L_{\mathrm{n}}^{\mathrm{s}}$ are the resistance and end-winding inductance of the n^{th} phase. The summation over i includes all the coil sides of phase n. Variable $\beta_{\mathrm{ni}} = \pm 1$ defines whether a positive or negative coil side is considered. N_{ni} is the number of turns and S_{ni} the cross-sectional are of coil side i. ℓ is the core length of the machine. The details of combining the field and circuit equations have been discussed among others in references [4]-[6]. A finite element method is used to solve the field and circuit variables numerically.

B. Impedance matrix

The aim is to present the circuit equations of the machine in matrix form

$$\underline{\boldsymbol{u}} = \underline{\boldsymbol{Z}}\,\underline{\boldsymbol{i}} \tag{4}$$

The dimensions of the impedance matrix $\underline{\boldsymbol{Z}}$ are $(m+Q_r)\times(m+Q_r)$, where m is the number of phases and Q_r the number of rotor bars. $\underline{\boldsymbol{u}}$ is a voltage vector and $\underline{\boldsymbol{i}}$ a current vector. The electromagnetic couplings between the windings can be uniquely defined only for a linear system. The linearization is done by solving the magnetic field in a chosen operation point and freezing the permeability of the iron core to this solution. Any of the field-circuit formulations referred to in Section II.A can be used to solve the linearization field.

The coupling impedances are obtained by inserting a current one by one in each phase winding and rotor bar and computing the voltages produced by this current in all the windings and bars. The current density in (2) must be expressed as a function of the total current. For instance, a current $\underline{i}_k$ in rotor bar k generates a magnetic vector potential $\underline{\boldsymbol{A}}$ according to equation

$$\nabla\times(\nu_0\nabla\times\underline{\boldsymbol{A}})+\mathrm{j}s\omega_s\sigma\underline{\boldsymbol{A}}-\mathrm{j}s\omega_s\frac{1}{S_k}\int_{S_k}\sigma\underline{\boldsymbol{A}}\cdot\mathrm{d}\boldsymbol{S}\;\mathbf{e}_z=\frac{\underline{i}_k}{S_k}\mathbf{e}_z \tag{5}$$

where ν_0 is the linearised reluctivity, s the slip, ω the supply frequency and S_k the cross-sectional area of the bar. The voltage induced in a stator phase winding is obtained from (3). The voltage over rotor bar n is

$$\underline{u}_n=\delta_{nk}R\,\underline{i}_k+\mathrm{j}s\omega_s\frac{\ell}{S_n}\int_{S_n}\underline{\boldsymbol{A}}\cdot\mathrm{d}\boldsymbol{S} \tag{6}$$

where the Kronecker symbol δ_{nk} assures that a resistive term is present only if the current and voltage are associated with the same conductor.

A element $\underline{z}_{nk}$ of the impedance matrix $\underline{\boldsymbol{Z}}$ is

$$\underline{z}_{nk}=\frac{\underline{u}_n}{\underline{i}_k} \tag{7}$$

The rotor voltage equation (6) is not in proper form for the impedance equation (4) as it does not include the voltages induced at the ends of the rotor cage. The missing terms can be taken into account by applying Kirchhoff's laws to the closed meshes of the cage. One possible method is discussed in [6]. When applied, the voltage equation for the rotor becomes

$$\underline{\boldsymbol{u}}^r=\mathbf{M}\underline{\boldsymbol{Z}}^{rs}\underline{\boldsymbol{i}}^s+(\mathbf{M}\underline{\boldsymbol{Z}}^{rr}+\underline{\boldsymbol{Z}}^{re})\underline{\boldsymbol{i}}^r=0\,. \tag{8}$$

The elements of matrices $\underline{\boldsymbol{Z}}^{rs}$ and $\underline{\boldsymbol{Z}}^{rr}$ are obtained from (6) and (7). Matrix $\underline{\boldsymbol{Z}}^{re}$ is associated with the end-winding impedances of the rotor cage. Matrix **M** transforms the bar voltages to mesh voltages.

C. Equivalent circuit for a single-cage motor

Fig. 1 shows the conventional T equivalent circuit. It represents the coupling between a stator phase current and a somewhat fictitious rotor current.

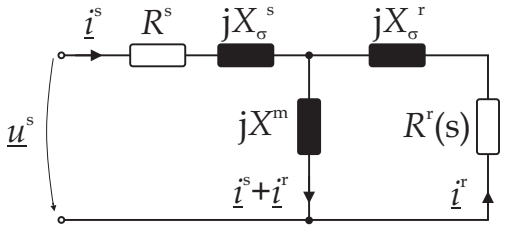

Fig. 1. Single-cage equivalent circuit model.

As there are two currents, the related coupling matrix $\underline{\boldsymbol{Z}}$ has dimensions 2×2. The approach of this study is to first compute the large impedance matrix including all the couplings as described in the previous section, and then reduce the large matrix to a 2×2 matrix associated with Figure 1. A method related to the symmetric components is used for the reduction. If the stator winding has m phases and the rotor bars are taken to form a poly-phase system with Q_r phases, the positive phase-sequence stator voltage, stator current and rotor current are defined

$$\begin{aligned}\underline{u}^s_+&=\frac{1}{m}\sum_{i=1}^{m}\underline{u}^s_i\mathrm{e}^{\mathrm{j}\frac{2\pi(i-1)}{m}}\\ \underline{i}^s_+&=\frac{1}{m}\sum_{i=1}^{m}\underline{i}^s_i\mathrm{e}^{\mathrm{j}\frac{2\pi(i-1)}{m}}\\ \underline{i}^r_+&=\frac{1}{Q_r}\sum_{i=1}^{Q_r}\underline{i}^r_i\mathrm{e}^{\mathrm{j}\frac{2\pi(i-1)}{Q_r}}\end{aligned}\,. \tag{9}$$

The subscript + refers to the positive phase sequence. By substituting the stator voltages from (4) in the first expression of Eq. (9), the positive phase-sequence voltage is obtained as a function of the phase and bar currents

$$\underline{u}^s_+=\frac{1}{m}\sum_{i=1}^{m}\sum_{k=1}^{m}\underline{z}^{ss}_{ik}\underline{i}^s_k\mathrm{e}^{\mathrm{j}\frac{2\pi(i-1)}{m}}+\frac{1}{m}\sum_{i=1}^{m}\sum_{k=1}^{Q_r}\underline{z}^{sr}_{ik}\underline{i}^r_k\mathrm{e}^{\mathrm{j}\frac{2\pi(i-1)}{m}} \tag{10}$$

where $\underline{z}^{ss}_{ik}$ refers to an element of the impedance matrix that couples two stator windings and $\underline{z}^{sr}_{ik}$ to an element that couples a stator winding to a rotor bar.

The first sum in (10) is taken to be the voltage induced by the positive phase-sequence stator current and the second sum the voltage induced by the positive phase-sequence rotor current. Based on this assumption, the equation is written in a simple scalar form

$$\underline{u}^s_+=\underline{z}^{ss}\,\underline{i}^s_++\underline{z}^{sr}\,\underline{i}^r_+ \tag{11}$$

where the impedances $\underline{z}^{ss}$ and $\underline{z}^{sr}$ are obtained by dividing the sum containing the stator currents by $\underline{i}^s_+$ and the sum containing the rotor currents by $\underline{i}^r_+$

$$\begin{aligned}\underline{z}^{ss}&=\frac{1}{m\,\underline{i}^s_+}\sum_{i=1}^{m}\sum_{k=1}^{m}\underline{z}^{ss}_{ik}\,\underline{i}^s_k\,\mathrm{e}^{\mathrm{j}\frac{2\pi(i-1)}{m}}\\ \underline{z}^{sr}&=\frac{1}{m\,\underline{i}^r_+}\sum_{i=1}^{m}\sum_{k=1}^{Q_r}\underline{z}^{sr}_{ik}\,\underline{i}^r_k\,\mathrm{e}^{\mathrm{j}\frac{2\pi(i-1)}{m}}\end{aligned}\,. \tag{12}$$

The positive phase-sequence rotor voltage is calculated in a similar manner as the stator voltage above

$$\underline{u}^r_+=\underline{w}^{rs}\,\underline{i}^s_++\underline{w}^{rr}\,\underline{i}^r_+=0 \tag{13}$$

The coefficients are

$$\underline{w}^{\mathrm{rs}} = \frac{1}{Q_{\mathrm{r}}\underline{i}_{+}^{\mathrm{s}}}\sum_{\mathrm{i}=1}^{Q_{\mathrm{r}}}\sum_{\mathrm{k}=1}^{m}\left\{\mathbf{M}\underline{\boldsymbol{Z}}^{\mathrm{rs}}\right\}_{\mathrm{ik}}\underline{i}_{\mathrm{k}}^{\mathrm{s}}\,\mathrm{e}^{\mathrm{j}\frac{2\pi(\mathrm{i}-1)}{m}}$$
$$\underline{w}^{\mathrm{rr}} = \frac{1}{Q_{\mathrm{r}}\underline{i}_{+}^{\mathrm{r}}}\sum_{\mathrm{i}=1}^{Q_{\mathrm{r}}}\sum_{\mathrm{k}=1}^{Q_{\mathrm{r}}}\left\{\mathbf{M}\underline{\boldsymbol{Z}}^{\mathrm{rr}}+\underline{\boldsymbol{Z}}^{\mathrm{re}}\right\}_{\mathrm{ik}}\underline{i}_{\mathrm{k}}^{\mathrm{r}}\,\mathrm{e}^{\mathrm{j}\frac{2\pi(\mathrm{i}-1)}{m}}\quad . \tag{14}$$

Equations (11) and (13) define the relation between the positive phase-sequence stator voltage and stator and rotor currents. As the equations have been derived from the voltage equations of two magnetically coupled poly-phase windings having different phase numbers, the coupling coefficients $\underline{z}^{\mathrm{sr}}$ and $\underline{w}^{\mathrm{rs}}$ are not equal. The equality is forced by rescaling (13)

$$\frac{\underline{z}^{\mathrm{sr}}}{\underline{w}^{\mathrm{rs}}}\left(\underline{w}^{\mathrm{rs}}\underline{i}_{+}^{\mathrm{s}}+\underline{w}^{\mathrm{rr}}\underline{i}_{+}^{\mathrm{r}}\right)=\underline{z}^{\mathrm{rs}}\underline{i}_{+}^{\mathrm{s}}+\underline{z}^{\mathrm{rr}}\underline{i}_{+}^{\mathrm{r}}=0 \tag{15}$$

where

$$\underline{z}^{\mathrm{rs}}=\underline{z}^{\mathrm{sr}}$$
$$\underline{z}^{\mathrm{rr}}=\frac{\underline{z}^{\mathrm{sr}}}{\underline{w}^{\mathrm{rs}}}\underline{w}^{\mathrm{rr}}\quad . \tag{16}$$

Equations (11) and (15) define a simple equivalent circuit of the single-cage induction motor. However, if leakage reactances are preferred, the rotor quantities have to be referred to the stator. A stator-referred rotor current flowing in the stator winding should induce a fundamental component of the air-gap flux that is equal to the fundamental component of the flux induced by the original rotor current. Using this criterion, a reference coefficient $\underline{\kappa}$ is obtained

$$\underline{\kappa}=\frac{\underline{\boldsymbol{\Phi}}^{\mathrm{s}1}\underline{i}_{+}^{\mathrm{r}}}{\underline{\boldsymbol{\Phi}}^{\mathrm{r}1}\underline{i}_{+}^{\mathrm{s}}} \tag{17}$$

where $\underline{\boldsymbol{\Phi}}^{\mathrm{s1}}$ and $\underline{\boldsymbol{\Phi}}^{\mathrm{r1}}$ are the fundamental components of the air-gap fluxes induced separately by the stator and rotor currents. The flux components are integrated from the air-gap vector potential. The parameters referred to the stator and marked by an apostrophe are

$$\underline{i}_{+}^{\mathrm{r}}{}'=\frac{1}{\underline{\kappa}}\underline{i}_{+}^{\mathrm{r}}$$
$$\underline{z}^{\mathrm{ss}}{}'=\underline{z}^{\mathrm{ss}}$$
$$\underline{z}^{\mathrm{sr}}{}'=\underline{\kappa}\underline{z}^{\mathrm{sr}}\quad . \tag{18}$$
$$\underline{z}^{\mathrm{rs}}{}'=\underline{\kappa}\underline{z}^{\mathrm{rs}}$$
$$\underline{z}^{\mathrm{rr}}{}'=\underline{\kappa}^{2}\underline{z}^{\mathrm{rr}}$$

The components of the equivalent circuit in Figure 1 are obtained from the impedances referred to the stator

$$R^{\mathrm{s}}=\mathrm{Re}\left\{z^{\mathrm{ss}}{}'\right\}$$
$$X_{\sigma}^{\mathrm{s}}=\mathrm{Im}\left\{z^{\mathrm{ss}}{}'-z^{\mathrm{sr}}{}'\right\}$$
$$X^{\mathrm{m}}=\mathrm{Im}\left\{z^{\mathrm{sr}}{}'\right\}\quad . \tag{19}$$
$$X_{\sigma}^{\mathrm{r}}=\mathrm{Im}\left\{z^{\mathrm{rr}}{}'-z^{\mathrm{rs}}{}'\right\}$$
$$R^{\mathrm{r}}=\mathrm{Re}\left\{z^{\mathrm{rr}}{}'\right\}$$

The linearization of the machine was done to a given operation point. The circuit parameters obtained are, of course, associated with the same operation point.

D. Multi-cage models

The method above can be generalised for a multi-cage machine or to a model in which the deep bars are divided in several sub-conductors. Such a division is shown in Fig. 2.

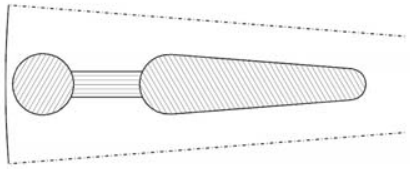

Fig. 2. Rotor bar is divided into three parts.

A positive phase-sequence rotor current is defined separately for each of the sub-conductor layers. If three sub-conductors per bar are used, the large impedance matrix is a $(m+3Q_{\mathrm{r}})\times(m+3Q_{\mathrm{r}})$ matrix, and (10), as an example, includes one sum for the stator currents and three sums for the positive phase-sequence sub-conductor currents. The reduction of the large impedance matrix leads to a 4×4 coupling matrix. Each rotor current is separately referred to the stator using (17). The circuit equation for the three-cage induction machine is of the form

$$\begin{pmatrix}u_{+}^{\mathrm{s}}\\0\\0\\0\end{pmatrix}=\begin{pmatrix}Z_{11}&Z_{12}&Z_{13}&Z_{14}\\Z_{21}&Z_{22}&Z_{23}&Z_{24}\\Z_{31}&Z_{32}&Z_{33}&Z_{34}\\Z_{41}&Z_{42}&Z_{43}&Z_{44}\end{pmatrix}\begin{pmatrix}i_{+}^{\mathrm{s}}\\i_{+}^{\mathrm{r1}}\\i_{+}^{\mathrm{r2}}\\i_{+}^{\mathrm{r3}}\end{pmatrix}. \tag{20}$$

Again, the 4×4 coupling matrix represents an equivalent circuit of the machine. However, multi-cage machines are often modelled using a ladder-type equivalent circuit. Such a circuit with three rotor branches is presented in Fig 3.

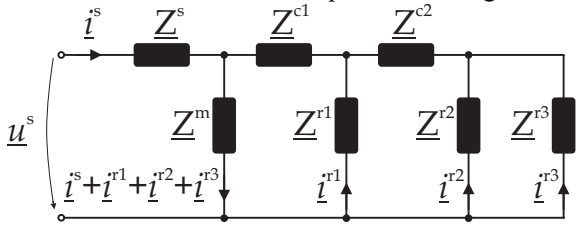

Fig. 3. Three-cage equivalent circuit model.

To fulfil Kirchhoff's second law in the circuit of Fig. 3, the coupling matrix should be of the form defined by (21) or at least, it should be possible to transform the system of equations (20) so that a coupling matrix of type (21) is obtained. Obviously, this is not possible for a general case. A 4×4 matrix has 12 elements but there are only 7 coefficients on the right hand side of (21). For the equality, the matrix on the left hand side must be symmetric.

$$\begin{pmatrix} Z_{11} & Z_{12} & Z_{13} & Z_{14} \\ Z_{21} & Z_{22} & Z_{23} & Z_{24} \\ Z_{31} & Z_{32} & Z_{33} & Z_{34} \\ Z_{41} & Z_{42} & Z_{43} & Z_{44} \end{pmatrix} = Z^{\mathrm{s}} \begin{pmatrix} 1 & 0 & 0 & 0 \\ 0 & 0 & 0 & 0 \\ 0 & 0 & 0 & 0 \\ 0 & 0 & 0 & 0 \end{pmatrix} + Z^{\mathrm{r1}} \begin{pmatrix} 0 & 0 & 0 & 0 \\ 0 & 1 & 0 & 0 \\ 0 & 0 & 0 & 0 \\ 0 & 0 & 0 & 0 \end{pmatrix} + Z^{\mathrm{r2}} \begin{pmatrix} 0 & 0 & 0 & 0 \\ 0 & 0 & 0 & 0 \\ 0 & 0 & 1 & 0 \\ 0 & 0 & 0 & 0 \end{pmatrix} + Z^{\mathrm{r3}} \begin{pmatrix} 0 & 0 & 0 & 0 \\ 0 & 0 & 0 & 0 \\ 0 & 0 & 0 & 0 \\ 0 & 0 & 0 & 1 \end{pmatrix} + Z^{\mathrm{m}} \begin{pmatrix} 1 & 1 & 1 & 1 \\ 1 & 1 & 1 & 1 \\ 1 & 1 & 1 & 1 \\ 1 & 1 & 1 & 1 \end{pmatrix} + Z^{\mathrm{c1}} \begin{pmatrix} 0 & 0 & 0 & 0 \\ 0 & 1 & 1 & 1 \\ 0 & 1 & 1 & 1 \\ 0 & 1 & 1 & 1 \end{pmatrix} + Z^{\mathrm{c2}} \begin{pmatrix} 0 & 0 & 0 & 0 \\ 0 & 0 & 0 & 0 \\ 0 & 0 & 1 & 1 \\ 0 & 0 & 1 & 1 \end{pmatrix} \tag{21}$$

Furthermore, the following constraints have to be fulfilled

$$\begin{aligned} &Z_{12} = Z_{13} = Z_{14} = Z_{21} = Z_{31} = Z_{41} = Z^{\mathrm{m}} \\ &Z_{23} = Z_{24} = Z_{32} = Z_{42} = Z^{\mathrm{m}} + Z^{\mathrm{c1}} \\ &Z_{43} = Z_{34} = Z^{\mathrm{m}} + Z^{\mathrm{c1}} + Z^{\mathrm{c2}} \end{aligned} \tag{22}$$

The diagonal elements are

$$\begin{aligned} &Z_{11} = Z^{\mathrm{s}} + Z^{\mathrm{m}} \\ &Z_{22} = Z^{\mathrm{r1}} + Z^{\mathrm{m}} + Z^{\mathrm{c1}} \\ &Z_{33} = Z^{\mathrm{r2}} + Z^{\mathrm{m}} + Z^{\mathrm{c1}} + Z^{\mathrm{c2}} \\ &Z_{44} = Z^{\mathrm{r3}} + Z^{\mathrm{m}} + Z^{\mathrm{c1}} + Z^{\mathrm{c2}} \end{aligned} \tag{23}$$

If the coupling matrix fulfils these constraints, the transformation to the ladder system is a straight forward process. If not, the ladder structure is too restrictive to describe the machine. When the coupling matrix (20) is constructed as described in Sections II-B–II-D, the conditions (22) are met very well, and the ladder-circuit parameters give almost exactly the same machine characteristics, i.e. stator current and torque, as the original FEM solution. This experience seems to apply for any division of the rotor bars to sub-conductors. Possible problems are discussed in Chapter IV.

III. Results

A 37-kW cage-induction motor is studied. Fig. 4 shows the geometry of the rotor and stator slots.

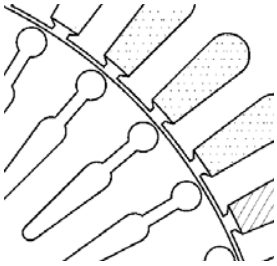

Fig. 4. Geometry of the stator and rotor slots.

Table I presents the rated values of the test motor.

TABLE I Rated values for the test motor.

P_N	[kW]	rated power	37
U_{sN}	[V]	rated stator voltage	380 (star)
p		number of pole pairs	2
f_N	[Hz]	rated stator frequency	50
s_N	[%]	rated slip	2.0

First, the effects of saturation are neglected when a FE model with a relative permeability of 1000 in the iron is studied. The model is referred as the linear FE model. However, the eddy currents in the rotor bars are included and therefore the parameters change along with the frequency. In all the performed computations, the temperature of the stator winding is 98 °C and rotor 135 °C.

The parameters of the single-cage circuit model are estimated at different slips. Using the obtained equivalent circuits, the torque versus speed curves are calculated. Fig. 5 presents the curves given by the equivalent circuits with the parameters calculated at slips 0.02, 0.5 and 1.0. They are compared with the torque obtained from the time-harmonic FEA at different operation points. Clearly, the single-cage equivalent circuit model predicts the torque adequately only near the same operation point where the parameters are estimated.

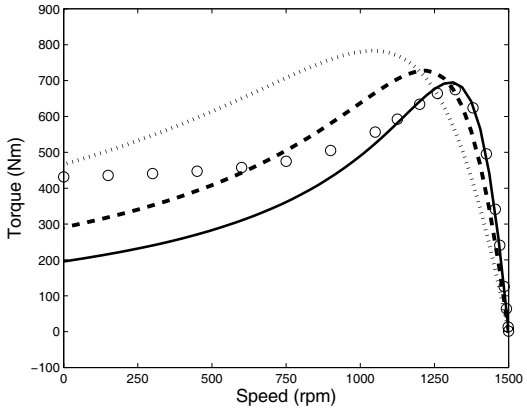

Fig. 5. Torque versus speed curves for the linearized motor. Solid line: s=0.02, dashed: s=0.5, dotted: s=1, circles: torque given by FEA.

Dividing the bar into three parts, a circuit model with two additional rotor branches is obtained. Fig. 6 presents the torque versus speed curves given by the three-cage equivalent circuit with parameters calculated at the three slips. The

torque is modelled more accurately in a wider operation range.

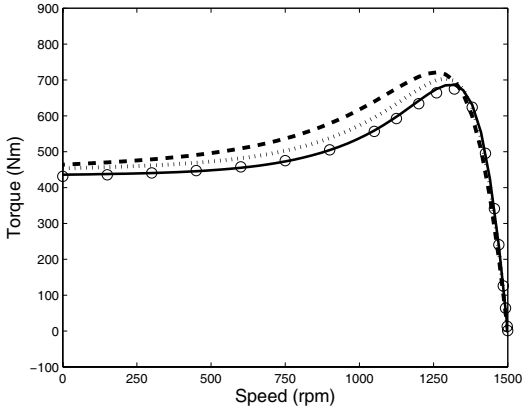

Fig. 6. Torque versus speed curves for the three-cage model (linear material). Solid line: s=0.02, dashed: s=0.5, dotted: s=1, circles: torque given by FEA.

Next, the permeability of the iron is allowed to depend on the flux density. This model is referred as the nonlinear FE model. Fig. 7 presents the torque versus speed curves calculated using three-cage circuit models with parameters obtained from the nonlinear FE model at different slips. Fig. 8 presents the corresponding stator currents.

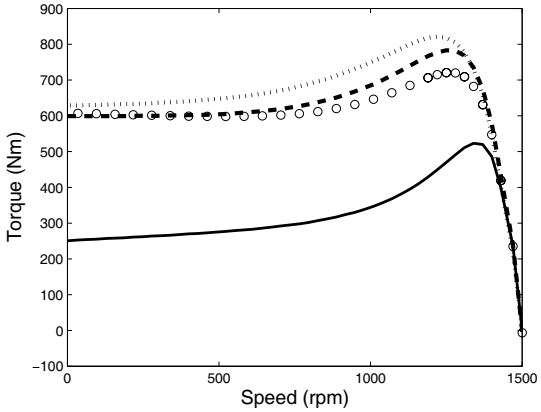

Fig. 7. Torque versus speed curves for the three-cage model (nonlinear material). Solid line: s=0.02, dashed: s=0.5, dotted: s=1, circles: torque given by FEA.

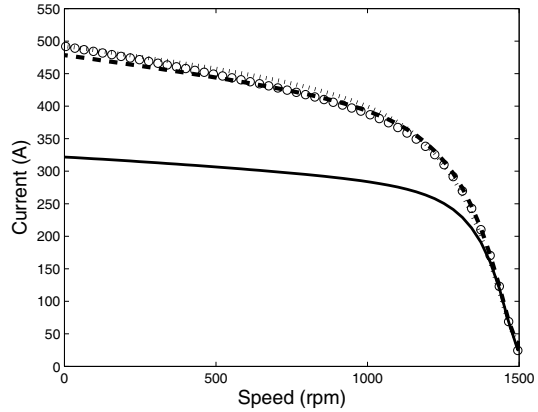

Fig. 8. Stator current given by the three-cage model (nonlinear material). Solid line: s=0.02, dashed: s=0.5, dotted: s=1, circles: torque given by FEA.

When the parameters are calculated at the rated slip the torque is modelled well only at the speed range between the rated-load and no-load. The parameters calculated at slips 0.5 and 1.0 provide more general results.

The parameters of the single-cage and three-cage models at the rated operation point are presented in Table II. The values of the resistances and inductances correspond to the real and imaginary part of the impedances presented in Fig. 3. The values of the resistances are to be divided by the slip when placed to the circuit model. The rotor parameters of the single-cage model (Fig. 1) are referred as R_{r1} and $X_{\sigma r1}$.

TABLE II PARAMETERS OF THE SINGLE-CAGE AND THREE-CAGE CIRCUIT MODEL AT RATED OPERATION POINT.

		1-cage	3-cage
R_s	[Ω]	0.08357	0.08357
$X_{\sigma s}$	[Ω]	0.2476	0.2463
X_m	[Ω]	8.431	8.432
R_{c1}	[Ω]	–	0.01537
X_{c1}	[Ω]	–	0.3153
R_{r1}	[Ω]	0.06681	0.2556
$X_{\sigma r1}$	[Ω]	0.4815	0.02419
R_{c2}	[Ω]	–	3.5400E-05
X_{c2}	[Ω]	–	0.1278
R_{r2}	[Ω]	–	0.4350
$X_{\sigma r2}$	[Ω]	–	0.03269
R_{r3}	[Ω]	–	0.07541
$X_{\sigma r3}$	[Ω]	–	0.1827

Since the saturation is modelled, the values of the parameters are affected by the supply voltage. Fig. 9 shows the magnetizing reactance of the three-cage circuit as a function of slip at supply voltages 240, 380, and 450 V. The voltage values correspond to the linear part of the magnetization curve, the rated operation point and a strongly saturated region.

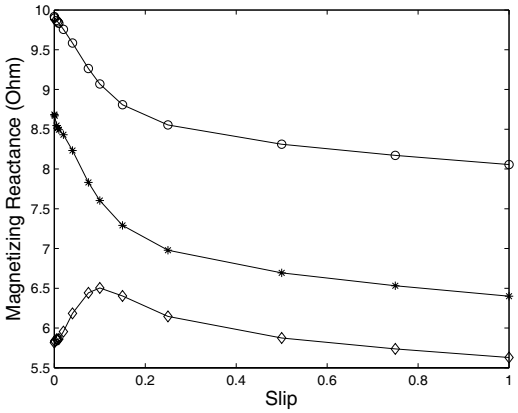

Fig. 9. Magnetizing reactance as a function of slip at the supply voltage 240 V (circles), 380 V (asterisk) and 450 V (diamonds).

The saturation affects mostly the value of the magnetizing reactance. Also, the values of the stator leakage reactance $X_{\sigma s}$ and rotor reactance X_{c1}, the largest reactance on the rotor side,

decrease when the supply voltage is increased. However, the value of the rotor reactance X_{c2} remains almost constant. The rotor reactance $X_{\sigma r3}$ increases slightly along with the supply voltage, but in practice the change is negligible. The values of the resistances are not influenced by the supply voltage, as expected.

The torque given by the time-harmonic FE analysis is also a simplification of the torque produced by the real induction motor. The torque as a function of speed has been measured at a reduced voltage of 320 V. The measurements are compared with the results of the FEA in Fig. 10.

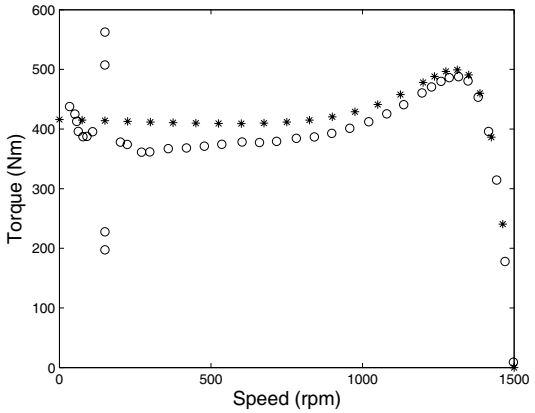

Fig. 10. Measured (circles) and simulated (asterisk) torque versus speed curves at the supply voltage 320 V.

IV. Discussion

The equivalent circuit model with three rotor branches is capable of modelling the torque in a wide speed range when the permeability of the iron is assumed to be constant. However, in the case of the nonlinear FE model the circuit parameters still depend quite strongly on the frequency. Only if the circuit parameters are calculated at large slips 0.5…1.0, the equivalent circuit can model the torque within a reasonable accuracy in the speed range from stand-still to no-load. Adding the number of the rotor branches up to seven does not significantly seem to improve the performance of the circuit model. Also, in the case of the linear model, circuit models with more than three rotor branches do not provide significantly better results.

When comparing the measured torque with the simulated one, the main difference is found at 150 rpm. The time-harmonic analysis fails in torque computation if there is a synchronous torque at zero speed. Otherwise the results are close to each other, especially at small slips. The effect of the rotor angle was studied by estimating the parameters for the rated operation point at different rotor angles. The differences between the parameters were found to be negligibly small. When the impedance matrix is constructed the obtained value for the stator resistance is about 10 % higher than the one given to the FE model. The stator resistance is corrected to correspond to the original value by moving the excess resistance to the rotor side. The modification does not change the performance of the circuit model.

The estimation results are difficult to evaluate through measurements since the parameters obtained from the conventional no-load and stand-still tests are not comparable with the parameters of the loaded operation point. However, the parameter estimates are physically reasonable in the sense how they behave as a function of supply voltage. The rotor resistances are not affected, but the reactances decrease along with the voltage, as expected.

At the large values of slip or at the low supply voltages some of the imaginary parts of the diagonal elements in (20) are somewhat smaller than the adjacent elements. They are related to the couplings between the rotor currents and therefore the estimated rotor reactances $X_{\sigma r2}$ and $X_{\sigma r3}$ can have small negative values. In that case, they are considered to be zero since the values of the resistances fully dominate the contribution of the branch. The phenomenon is a subject for further studies.

V. Conclusions

The parameters of the deep-bar induction motor are greatly influenced by the skin effect in the rotor bars. Therefore the traditional single-cage model fails in predicting the torque versus speed curves. The circuit model with additional rotor branches gives better results. However, if the saturation of the iron is modelled, the parameters become more dependent on the frequency. The parameters estimated at the large slips model the torque on a wider operation range. The parameters given by the presented method are related to the effective permeability of the iron. Therefore they are suitable for modelling the steady-state operation of the electrical machine. Such parameters can be used in design and simulation of electric drives.

References

[1] A. C. Smith, ,R. C. Healey, and S. Williamson, “A Transient Induction Motor Model Including Saturation and Deep Bar Effect,” *IEEE Trans. on Energy Conversion*, vol. 11, pp. 8-15, March 1996.

[2] S. D. Sudhoff, D. C. Aliprantis, B. T. Kuhn, and P. L. Chapman “An Induction Machine Model for Predicting Inverter-Machine Interaction,” *IEEE Trans. on Energy Conversion*, vol. 17, pp. 203-210, June 2002.

[3] J. Luomi, A. Niemenmaa, A. Arkkio, “On the use of effective reluctivities in magnetic field analysis of induction motors fed from a sinusoidal voltage source,” in *Proc. of the International Conference on Electrical Machines*, München, 1986, vol. 2, pp. 706–709.

[4] E. G. Strangas, and K. R. Theis, “Shaded pole motor design and evaluation using coupled field and circuit equations,” *IEEE Trans. on Magnetics*, vol. 21, pp.1880–1882, September 1985.

[5] D. Shen, G. Meunier; J. Coulomb; and J. Sabonnadiere, “Solution of magnetic fields and electric circuits combined problems,” *IEEE Trans. on Magnetics*, vol. 21, pp.2288–2291, November 1985.

[6] A. Arkkio, “Analysis of induction motors based on the numerical solution of the magnetic field and circuit equations,” Doctoral Thesis, Acta Polytechnica Scandinavica, Electrical Engineering Series, no. 59, Helsinki, 1987, 97 p. Available: http://lib.hut.fi/Diss/198X/isbn951226076X